

X-Ray Interferometry at ESRF Using Two Coherent Beams from Fresnel Mirrors

K. Fezzaa,^{*,1} F. Comin,^{*} S. Marchesini,[†] R. Coïsson,[†] and M. Belakhovsky[‡]

^{*}European Synchrotron Radiation Facility (ESRF), Avenue des Martyrs, BP 220 38043 Grenoble Cedex, France; [†]University of Parma and Istituto Nazionale di Fisica della Materia, via M d'Azeglio 85 43100 Parma, Italy; and [‡]Département de Recherche Fondamentale sur la Matière Condensée, Service de Physique des Matériaux et Microstructures, CEA/Grenoble 17, rue des Martyrs, 38054 Grenoble Cedex 9, France

Received May 30, 1996

Using two small flat mirrors under grazing incidence, we have produced interference patterns from partially coherent x-ray beams at the European Synchrotron Radiation Facility. By piezoelectrically orienting one mirror around the horizontal plane, both the vertical and horizontal transverse coherence distances of the radiation have been measured. The experimental setup can be used to characterize the coherence properties along x-ray synchrotron beamlines. © 1997 Academic Press

INTRODUCTION

The European Synchrotron Radiation Facility (ESRF, Grenoble) is an optimized x-ray ring of the third generation. A specific characteristic of these sources is the small electron emittances; starting from the nominal horizontal value of 7 nm and a 10% coupling, a dramatic improvement has recently been achieved. The new settings correspond to 4 nm and 1% coupling, without compromising the other parameters such as lifetime, intensity, and stability (*I*). Besides boosting the brilliance by two orders of magnitude compared with the original ESRF specifications, these improvements increase accordingly the coherent flux in the x-ray domain.

Using the wavefront division method at the “SEXAFS and Standing Waves” beamline (ID32 at ESRF), we have already reported on the first interferometric tests in the hard x-ray domain using grazing incidence mirrors (2). Other authors have previously used Fresnel mirrors in soft x-rays for measurements of the refractive index (3). We have introduced several improvements to the original setup as well as to the experimental conditions. In the following, far better results are presented which demonstrate the validity of our approach as a methodological tool for characterizing the source itself as well as components along a beamline (some results on beam filtering will be discussed at a later stage). In particular, we have obtained the vertical coherence distance, and for the first time the horizontal coherence distance.

The spatial coherence of an optical wavefront, defined quantitatively by the “mutual intensity function” (referred hereafter as MI), can be experimentally determined (and

¹ E-mail: fezzaa@esrf.fr.

is in fact operationally defined) by Young's experiment with a variable slit separation. For an x-ray beam it might be more convenient to use reflecting optics, because two thick slits with a short and variable distance between them are difficult to realize and their edges reflect and add spurious radiation to the interference pattern. Although mirrors are never ideally flat, imperfections hardly affect the central zone in the extreme Fresnel (or Fraunhofer) domain. Moreover, the mirror setup has more degrees of freedom and we will show that with two almost horizontal small mirrors it is possible to measure the x-ray transverse coherence properties.

We will describe in the first section the setup and the experimental results. Then the theoretical model is given in Section 2 and compared with experimental results in Section 3. Finally, some conclusions and perspectives are offered.

1. EXPERIMENTAL

1.1. Description of the Experiment

On the "SEXAFS and Standing Waves" beam line at the ESRF, two undulators with 40- and 48-mm periods, respectively, are inserted in the ID32 high β straight section. This beamline is very appropriate for coherent studies since it is windowless; therefore the wavefront is not perturbed and a wide range of suitable energies is available. Using a Si double crystal monochromator (with adequately polished crystals), experiments can be performed with high flux down to quite low energies (≈ 2.2 keV). The setup is similar to the one used previously (2), but is lighter and smaller, containing only two mirrors instead of four. These are small square silicon mirrors of 1 cm on a side and with high surface quality, less than 1-nm rms roughness and less than 4-arcsec rms slope error for both mirrors, and convex warpings of 0.6 and 0.8 μm , respectively. In order to insure that the reflecting surfaces of the mirrors lie in the same plane (within the stroke of the piezosystem described below), *ex situ* alignment was accomplished by letting the two mirrors flatten against a well polished silicon flat and glueing their back with wax to the support. One mirror can be actuated through a three-legged piezosystem of ≈ 0.6 mrad angular stroke and a maximum 7 μm vertical translation (4); one volt (upon the maximum value of 75 V) on a given piezo corresponds to 45 nm or 8 μrad in angle. The double mirror system is inserted in a small UHV chamber, itself incorporated into the beamline at a distance of $D_1 = 30$ meters from the source and 3 meters downstream from the monochromator, inside the optical hutch of the beamline. This baby chamber rests on a cradle that has the same degrees of freedom as the piezoactuators (vertical translation and two orthogonal tilts); in addition, an underlying transverse translation stage moves the mirrors laterally with respect to the beam. The setup is shown in Fig. 1, where the piezoactuated mirror denoted by m_1 is the one located downstream. The (x, y, z) reference frame is with the y -axis along the beam, the z -axis being vertical (oriented upwards) and the x -axis being horizontally transverse (positive towards the storage ring). Since the typical incidence angles on the mirror system are in the milliradian range, the beams are totally reflected from the mirror surfaces. They are detected downstream at $D_2 = 15.7$ meters in the experimental hutch, using a NaI scintillation detector mounted in air behind a fine slit (5 or 1.5 μm of vertical aperture); both the detector and the slit can

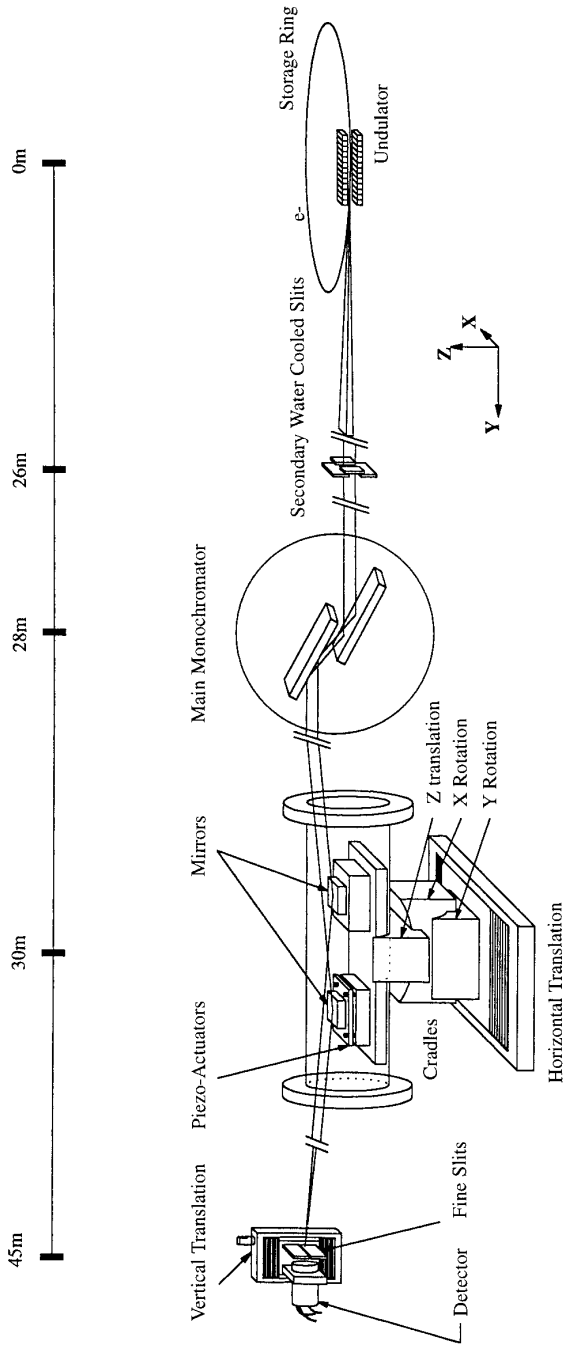


FIG. 1. General sketch of the Fresnel mirrors experiment.

TABLE 1
Typical Experimental Conditions

Source vert. size & emittance ^a	Undulator period and gap	Secondary slits	Monochromator	Mirrors	Distances	Detection slit
$\epsilon_v \approx 0.21 \text{ nm}$ $\sigma_v \approx 150 \text{ } \mu\text{m}$	$p = 48 \text{ mm}$ $g = 40 \text{ mm}$	$S_v = 60 \text{ } \mu\text{m}$ $S_H = 20 \text{ } \mu\text{m}$	Si (111) 6 keV	$L_y = 8.8 \text{ mm}$ $d_y = 58 \text{ mm}$	$D_1 = 30 \text{ m}$ $D_2 = 15.7 \text{ m}$	$5 \text{ } \mu\text{m}$

^a As provided by the machine group.

rotate with millidegree resolution around the x -axis and translate (with micrometer resolution) along the z - and x -axes.

The rotation allows us to orient the slit parallel to the incoming beam, and the vertical MI is sampled using z (height) scans. An x-ray camera can alternately be used to visualize and record the beam image. Upstream from the monochromator (two Si[111] crystals, liquid nitrogen cooled), a double pair of cross slits (cf. Table 1 and Fig. 1) limit the heat load on the optics and also avoid saturation of the NaI detector. Removable fluorescent screens can be inserted in the beam either downstream of the mirrors or further down, in order to quickly locate the different beams (direct, reflected, or refracted) and to align them in the same vertical plane (yz). The fine detector slit is set parallel to the x -axis. The whole system is in the same vacuum as the storage ring itself up to a beryllium window located in front of the detection system.

1.2. Experimental Results

Unless otherwise stated, the experimental conditions are those given in Table 1 (cf. Fig. 1 and 4), which gathers the geometric and spectral characteristics of the x-ray beam along its path (i.e. from source to detector). It is important to note that no harmonic contamination was present thanks to a strong detuning of the two crystals of the monochromator (also dictated by the saturation of the detector).

We will select below some results in order to illustrate three aspects that clearly demonstrate the efficiency of the experimental setup: first, in the vertical plane, the progressive overlap of the two reflected beams; then the probing of the vertical coherence; and finally, the probing of the horizontal coherence.

1.2.1. Progressive overlap of the reflected beams. The initial settings are such that there is no transverse tilt of the mirrors, i.e., the scattering geometry is purely vertical. Figure 2 shows x-ray camera images of the beams reflected by the two mirrors, first before overlap (a) and after full overlap (b). In particular, in Fig. 2a the outer Fraunhofer zones are clearly visible between the two central zones. More detailed information can be obtained from height scans of the detector. Figure 3a represents such a scan, showing the two beams that have been totally reflected from the two mirrors; the grazing angle α_0 on the m_2 mirror can be determined with accuracy by detecting at the distance D_2 the direct beam (mirror setup escamoted) and the reflected pair (since the angle between the direct beam and the center of the diffraction pattern

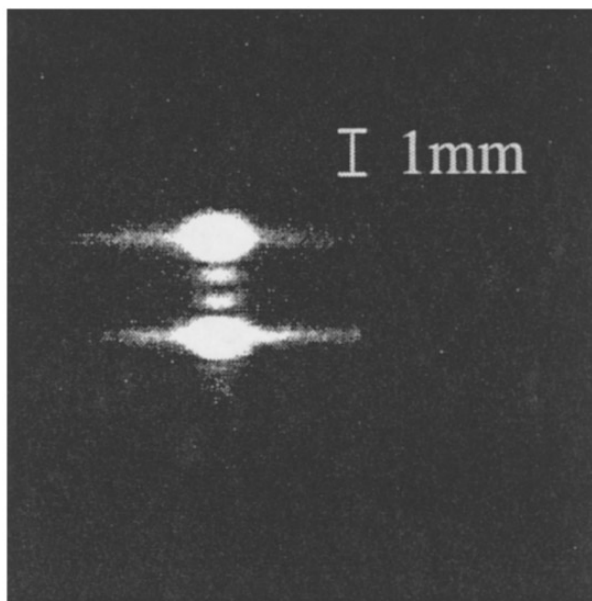
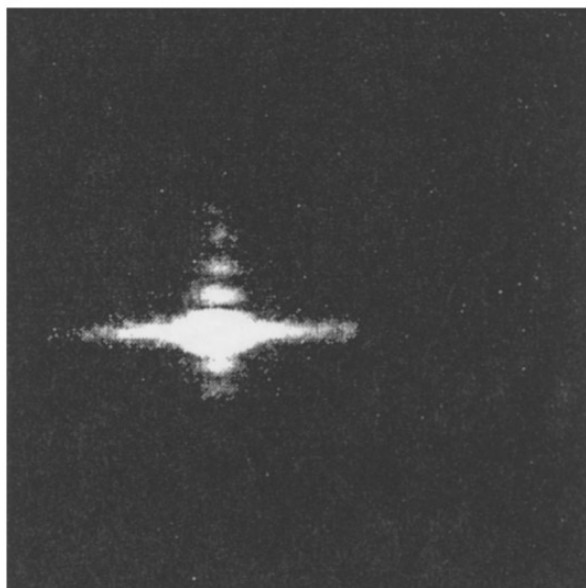
a**b**

FIG. 2. X-ray camera images of the reflected beams (a) before overlap, and (b) full overlap.

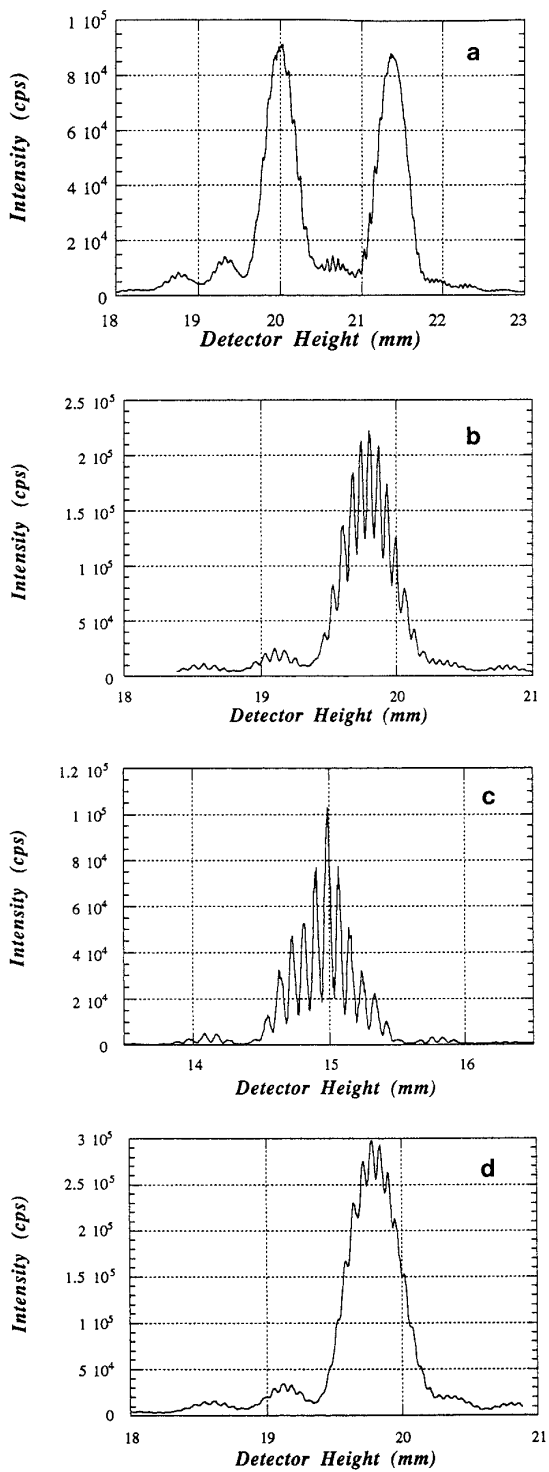


FIG. 3. Progressive overlap of the 2 reflected beams (a), and changes of grazing angle (b, c) and of transverse tilt (b, d).

from m_2 is twice the grazing angle); in Fig. 3, the zero of height ($z = 0$) corresponds to the direct beam position.

The widths of the two beams are ≈ 0.6 mm, although slightly unequal, mainly due to the different warping of the mirrors. In addition to the Fraunhofer pattern from each individual mirror, the proximity of the two beams already manifests itself by the interference modulations that appear on these patterns. By progressively changing the voltage of the relevant piezo, the beam reflected by m_1 is moved toward the m_2 beam at the detector location until complete overlap is reached, the resulting pattern being shown in Fig. 3b. Considering each mirror as a slit of width $a' = \alpha L_y \approx \alpha_0 L_y$ (where the prime indicates a value from the detector side (cf. Fig. 4) and $\alpha = \alpha_0 + z/D_2$), the expected height Δz of the central lobe should be $\Delta z \approx \lambda D_2/a'$; in the case of Fig. 2b, $\alpha_0 \approx 0.7$ mrd and $a' \approx 5 \mu\text{m}$, hence $\Delta z \approx 0.6$ mm, as seen in the figure. Several zones are shown in Fig. 2, all modulated by the interference effect between the two coherent subbeams. The detector slit and the scan step ($5 \mu\text{m}$, in general) have been defined in order to sample with at least 10 points each interference fringe. The number of these fringes are related to the ratio of the interspacing between the mirrors d_y with respect to their size L_y (cf. Fig. 4); for instance, in Fig. 3b again, the projected distance between the mirrors as seen from the detector is $d'_z \approx \alpha_0 d_y = 32 \mu\text{m}$ and the interfringe spacing is $\lambda D_2/d'_z \approx 100 \mu\text{m}$, in agreement with the data. There is a marked asymmetry in the modulations between the right and left sides of the central zone; this is due to the fact that the mirrors are not the usual Young slits (i.e., normal to the beam), but rather are inclined slits.

1.2.2. Effect of a change in the x-ray energy. With the settings of the piezos for complete overlap, and with no transverse tilt of the mirrors, the height scans of the detector are now performed for two different energies (6.20 and 4.35 keV). The results are shown in Figs. 3b and 3c: the major modification is the visibility increase by nearly a factor two (from 30 to 58%). This directly reflects the change in the transverse coherence, which is proportional to the wavelength.

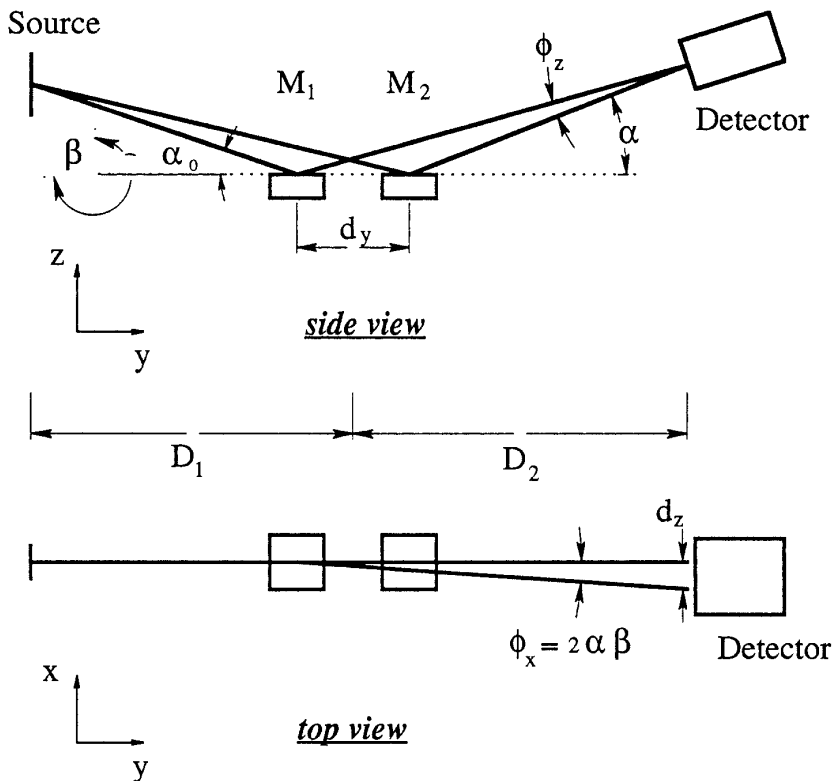
Similar considerations hold when varying the incidence angle α_0 , which is equivalent to sampling different vertical coherence distances.

1.2.3. Effect of a transverse tilt. We consider now a fixed grazing angle $\alpha_0 = 0.66$ mrd. The piezoactuated mirror m_1 is tilted transversely, i.e., around the y -axis (propagation direction) by ≈ 0.5 mrd. It is readily seen that the visibility of the interference fringes is drastically reduced from the zero transverse tilt (Fig. 3b) to the 0.5 mrd tilted one (Fig. 3d). This is because in this latter case the horizontal coherence (much smaller at our beamline location than the vertical coherence) now enters into play, as can be understood from the following section.

2. THEORETICAL MODEL

The relationship between two points p_1 and p_2 of the same transverse plane at location y along the x-ray path can be expressed by the so-called mutual intensity function (MI), which is the correlation function of the complex envelope of the wave $f_y(p_1)$,

$$M f_y(p_1, p_2) = \langle f_y^*(p_1), f_y(p_2) \rangle, \quad [1]$$



$\{ M_1(\text{piezoactuated}), M_2 \}$: Small mirrors
 $\{ \alpha, \alpha_0 \}$: grazing angles
 β : tilt angle of one mirror
 ϕ_z : convergence angle, ϕ_x : horizontal deflection

FIG. 4. Setup geometry.

where $\langle \dots \rangle$ indicates an ensemble average, or by the coherence degree μ which is the normalized MI.

The synchrotron radiation will be approximated here by a Gauss-Schell beam (6). The x rays impinge onto the two mirrors m_1 and m_2 with a vertical cross section

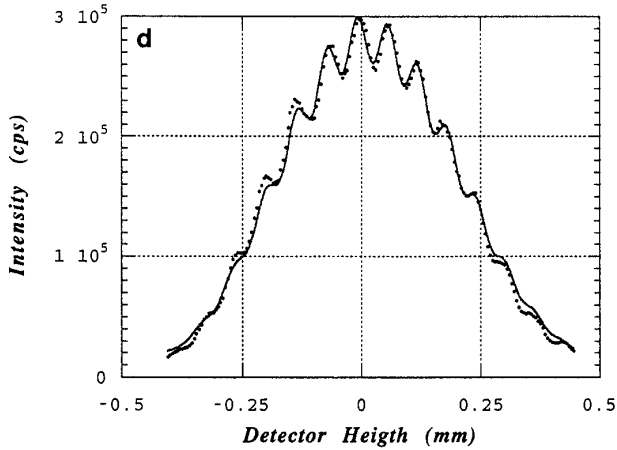
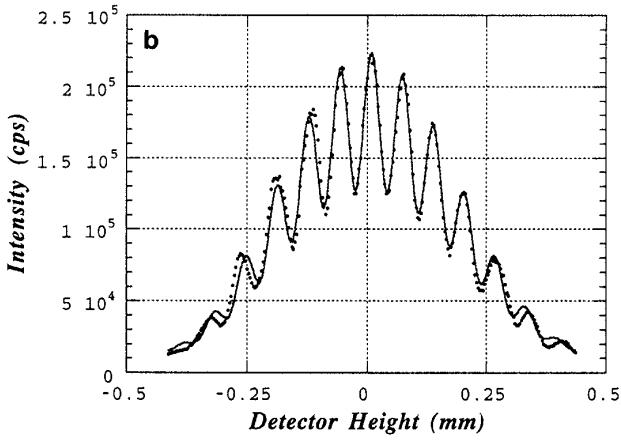
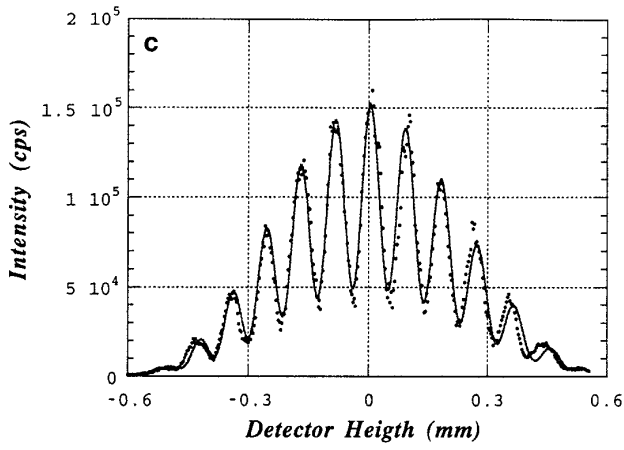


FIG. 5. Experimental spectra (dots) and fits (continuous lines) using the model described in Section 2.

distance $d_z \approx \alpha_0 d_y$. Assuming a transverse tilt β of the piezoactuated mirror m_2 , the corresponding beam is deflected by $\phi_x = 2\alpha\beta$, leading to a lateral displacement d_x at the detector location (cf. Fig. 4 for the definition of the geometrical parameters). Since the diffracted beam width at the detector is in the millimeter range for the central zone considered here, the effective mirror size as seen from the detector a' is $\approx 5 \mu\text{m}$ and $d'_z \approx 30 \mu\text{m}$; hence we can use the far field approximation, since $\exp\{ik a'^2/D_2\} \approx 1 + 0.05 i$.

In the experimental setup, the vertical coherence size $\hat{\sigma}_{cz}$ at the mirrors being larger than the mirror cross section, the quantities $\exp\{-a'^2/2\hat{\sigma}_{cz}^2\} \cong 0.994$ and $\exp\{-ad_z/2\hat{\sigma}_{cz}^2\} \cong 0.9$ have been replaced by unity (the last approximation is not necessary but simplifies the solution). This leads to an analytical solution in far field:

$$I_{\text{det}}(x, z) = I_0 \left| \sin c \left(\frac{D_2 z}{a' \lambda} \right) \right|^2 \left[1 + V \cos \left(\frac{2\pi}{\lambda} \phi_z z + \frac{2\pi}{\lambda} \phi_x x + \varphi_0 \right) \right]. \quad [2]$$

In this expression of standard form, I_0 is the peak intensity reflected by each mirror and ϕ_z is the angle subtended by the two mirrors at the detector. The fringe phase φ_0 depends on the position of the mirror with respect to the center of the beam and on the difference in height and tilt between the mirrors; φ_0 is irrelevant to determining the properties of the beam.

The visibility V (or contrast) can be written in the case of a Gauss–Schell beam as

$$V \equiv \mu_{\text{mir}}^\nu(d_z) \mu_{\text{det}}^h(d_x) = \exp \left(-\frac{1}{2} \left(\frac{d_x}{\hat{\sigma}_{cx}} \right)^2 \right) \exp \left(-\frac{1}{2} \left(\frac{d_z}{\hat{\sigma}_{cz}} \right)^2 \right), \quad [3]$$

where $\hat{\sigma}_{cx}$ is the horizontal coherence size at the detector location.

The visibility of the fringes depends on the coherence in both transverse directions: in the vertical direction the coherence between two points separated by a distance d_z is probed at the mirrors location, whereas the horizontal coherence is probed at the detector location and for a separation d_x . The orientation of the fringes is inclined by an angle $\arctan(\phi_x/\phi_z)$ relative to the horizontal direction, as if the two beams were coming from two different directions. For the sake of clarity the above presentation has been somewhat oversimplified; in actual calculations we have taken in account a slightly enhanced visibility at the center as well as the variation of a' , d'_z , and ϕ_z with the point of observation.

3. FIT AND RESULTS

The main results are summarized in Table 2, which gathers some typical cases of grazing angles, two for a zero transverse tilt between the two mirrors and one with a 0.5-mrd tilt.

The fitting procedure has been done with the parameter set $(I_0, \varphi_0, \alpha_0, \sigma_c, I_n)$ corresponding respectively to the peak intensity of each reflected beam, the phase of the fringes, the grazing angle of incidence, the coherence distance, and the mean noise

TABLE 2
Selected Results

Scan (cf. Figs. 3 & 5)	c	b	d (tilt = 0.5 mrd)
Wavelength λ (Å)	2.85	2.0	2.0
Grazing angle α_0 (mrd)	0.83	0.79	0.78
Visibility V (%)	52 ± 5	30 ± 2	7 ± 1
Coherent dist. σ_c (μm)	43 ± 4	25 ± 3	assumed to be the same as scan b
Horizontal coherence σ_h (μm)			7 ± 3

(see below). The estimated values were found by minimizing the rms error between the theoretical and the experimental intensities. The estimated error was calculated by equating the average variation of the theoretical intensity due to a variation of the parameters (given by the second order term in the Taylor expansion since the first one was zero because the fitted parameters were at the minimum) to the average error of the intensity (9).

Because of insufficient information on the position of the direct beam, it was necessary to deduce the angle of incidence α_0 from the numerical fit; this was done by relating the beam size to the projected mirror size $a' = \alpha L_y$ and the fringe frequencies to the mirrors' projected distance. The results showed that the effective distance d_z was related only to the horizontal separation of the two mirrors, hence confirming the approximate coplanarity of the two mirror surfaces. The distance δ_z between the mirror planes, as determined by the fit, is $\delta_z = (0 \pm 4) \mu\text{m}$. Since the cross-section distance as seen by the detector is $d'_z \approx d_z + 2\delta_z$ ($\alpha \approx \alpha_0$), this increases the error in d_z estimated with $\delta_z = 0$. Taking this into account, the uncertainty in the value of the coherence distances were approximately three times the ones indicated in Table 2. This error can be easily reduced to a negligible value, since the angle α_0 is well defined experimentally.

At the time of the experiment, the coupling constant of the storage ring was not optimized (5%). The emittances and optical β -functions were given (by the ESRF machine group) for the ID32 beamline location as $\epsilon_v = 0.20 \pm 0.2 \text{ nm}$, $\beta_v = 13.3 \pm 1.4 \text{ m}$, $\epsilon_H = 3.8 \pm 0.2 \text{ nm}$, and $\beta_H = 26 \pm 3 \text{ m}$. From these data, we deduce the source sizes $\sigma_H^s = 314 \mu\text{m}$ and $\sigma_v^s = 51 \mu\text{m}$, and hence the corresponding coherence distances at $\lambda = 2\text{\AA}$:

$$\sigma_c^v = \frac{\lambda D_1}{2\pi\sigma_v^s} \approx 20 \mu\text{m}; \quad \sigma_c^H = \frac{\lambda^*(D_1 + D_2)}{2\pi\sigma_H^s} \approx 4 \mu\text{m},$$

with 15% uncertainty.

These values are somewhat smaller than ours (cf. Table 2). This can be ascribed to the presence of slits upstream from the monochromator: in the vertical plane, a $60\text{-}\mu\text{m}$ slit width increases by a factor of 1.2 the coherence size. The same trend arises in the horizontal plane, but the effective size of the slit was not known with precision.

4. CONCLUSION

We have determined the transverse vertical coherence for various wavelengths, using our double mirror setup on the ID32/BL13 beamline at ESRF. In addition, and for the first time, we also determined the horizontal coherence. Comparison with the storage ring electron beam size is reasonable, given the accuracy of the electron beam parameters.

As the coherence distances are still much smaller than the beam widths, the field can be considered “quasi-homogeneous” (5); in this case, as shown in (7), the Van Cittert–Zernike theorem is applicable. With a further decrease of the vertical emittance and possibly with a lower beta function (both being underway at the ESRF), or with a longer wavelength, it might be possible to verify the deviations from it, as was foreseen in (7).

The practical interest of the presented setup is not only to monitor the source quality itself, but also to obtain information downwards: the coherence properties along the x ray might be degraded in a way that cannot be quantitatively predicted. For example, we have obtained preliminary data which show that carbon filters inserted along the x-ray beam path clearly alter the interference pattern; such degradations have also been pointed out previously in the case of standard ESRF beryllium windows (8). Apart from this diagnostic aspect, our setup could also be used in the field of surface physics, e.g., for studying deposits (such as mesoscopic systems) on one mirror, with the other mirror serving as a reference wave.

ACKNOWLEDGMENTS

We express our thanks for their contribution to all members of the ID32/BL13 staff, as well as to Peter Kamp. Also, we express our gratitude to the ESRF management who gave approval for the present experiment during the commissioning phase of the beamline.

REFERENCES

1. L. Farvacque, J. L. Laclare, C. Limborg, and A. Ropert, *ESRF Newslett.* **24**, 12 (1995).
2. M. Belakhovsky, R. Coisson, F. Comin, P. Kamp, S. Marchesini, and K. Fezzaa, in “Surface. X-Ray Synchrotron and Neutron Investigations, Proceedings of IPX-95, Moscow, Aug. 1995,” Vols. 3/4, Russian Acad. of Sciences, Moscow, 1996.
3. J. Svatos, D. Joyeux, D. Phalippou, and F. Polack, *Opt. Lett.* **18**, 1367 (1993).
4. NanoFlex 17 ASM 003 from Melles-Griot.
5. J. W. Goodman (Ed.), “Statistical Optics,” Wiley–Interscience, New York, 1985.
6. E. Wolf and E. Collet, *Opt. Comm.* **25**, 293 (1978); H. P. Baltes and B. Steinle, *Nuovo Cimento B* **41**, 430 (1977); and Ref. (7) below.
7. R. Coisson, *Appl. Opt.* **34**, 904 (1995).
8. A. Snigirev, I. Snigireva, V. Kohn, and S. Kuznetsov, *Nucl. Instrum. Methods* (1996).
9. *Phys. Lett. B* **239** (1990).